

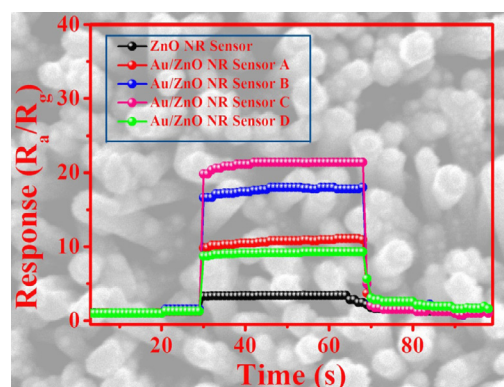
Highly sensitive gold-decorated zinc oxide nanorods sensor for triethylamine working at near room temperature



Xiaopan Song, Qi Xu, Hongyan Xu, Bingqiang Cao*

Materials Research Center for Energy and Photoelectrochemical Conversion, School of Materials Science and Engineering, University of Jinan, Jinan 250022, Shandong, China

GRAPHICAL ABSTRACT



ARTICLE INFO

Article history:

Received 8 February 2017

Revised 20 March 2017

Accepted 20 March 2017

Available online 27 March 2017

Keywords:

Au/ZnO nanorods

TEA sensor

Near room temperature

Schottky contact

ABSTRACT

There is an increasing worldwide demand for chemiresistive sensors for specific gas working at low temperature, in particular for standalone and mobile systems, which call for small and low power devices. In this paper, we successfully assemble highly sensitive triethylamine (TEA) gas sensors working at near-room temperature with gold (Au)-decorated ZnO nanorods. ZnO nanorods grow directly on flat Al_2O_3 ceramic electrodes by a cost-effective hydrothermal method and Au nanoparticles are deposited onto ZnO nanorods by DC-sputtering. Au-loaded ZnO (Au/ZnO) nanorods sensor at working temperature of 40°C and relative humidity of 30% exhibits high response (22–50 ppm TEA), low detection concentration (~ 1 ppm), and short response/recovery time (11 s/15 s), which are all much better than the pristine ZnO nanorods sensor. When the relative humidity increases, the sensor response decreases due to the water molecules adsorption. Moreover, the enhanced sensing properties of the Au/ZnO sensors are discussed in detail with the semiconductor depletion layer model introduced by the Au/ZnO Schottky contact and the catalytic effect of noble gold nanoparticles.

© 2017 Elsevier Inc. All rights reserved.

1. Introduction

Triethylamine (TEA), as a kind of important organic amine, has widespread applications including catalyst, organic solvent, high

energy fuel, preservative, and bactericide [1–4]. It is also one of the toxic gases released from harvested fishes and sea creatures during their deterioration process [5,6]. TEA is harmful to human body and can cause irritations to the dermal, ocular, and respiratory systems. In addition, long-term exposure to TEA may eventually result in abnormal embryos [7–9]. Several methods have been adopted to detect TEA, such as gas chromatography, ion mobility

* Corresponding author.

E-mail address: mse_caobq@ujn.edu.cn (B. Cao).

spectrometry, and liquid chromatography [10–12]. But, these traditional detecting methods are usually time-consuming due to complex operating process [10,13]. Therefore, it is still a strong demand to develop convenient, fast, and on-line TEA detecting method with high selectivity and sensitivity.

Semiconducting metal oxide nanostructures offer a promising platform for gas sensors with several advantages in terms of low cost, simple fabrication, and good compatibility with microelectronic processes [1]. Zinc oxide (ZnO) is a typical n-type semiconductor with a direct wide band gap of 3.37 eV at room temperature [14–18]. ZnO nanostructures such as nanowires [19], nanorods [20,21], and nanotubes [22] have been demonstrated for sensor applications with high sensitivity due to their large specific surface area, less agglomerated configuration, and high crystallinity [23]. Particularly, they have exhibited good sensing property to C_2H_5OH [18], CO [21], NH_3 [24], H_2S [25], and so on. For TEA gas sensor applications, Zhang et al. [26] fabricated ZnO nanorods sensor to detect TEA at 270 °C. Then, our group prepared ZnO nanosheets to detect TEA and obtained high response (78.4 for 50 ppm) and fast response time (6 s) at 320 °C [27].

Moreover, noble metal nanoparticles have been adopted to decorate semiconductors to improve their gas sensing properties such as sensitivity, selectivity, and response time. Au nanoparticles are typical noble metal with advanced optical, electrical, and catalytic properties [28,29]. Au nanoparticles modified ZnO nanostructures have been used to enhance the sensing performance of semiconductor chemiresistive gas sensor. For instance, Li et al. [30] reported Au@ZnO yolk-shell nanospheres to detect 100 ppm acetone and the response was about 2–3 times higher than that of ZnO hollow nanospheres at 300 °C. Majhi et al. [31] prepared Au@ZnO core-shell nanoparticles, which exhibited better selectivity to H_2 than pure ZnO nanoparticles. Zou et al. [32] developed a solution combustion method for the synthesis of Au/ZnO nanostructure, which also exhibited good sensitivity and fast response time (3 s) toward acetone at 300 °C. Generally, the ZnO TEA gas

sensor usually works at temperature as high as 250–400 °C [33]. This leads to high power consumption and fast device failure. Moreover, high temperature may result in the ignition of flammable and explosive target gases. Therefore, the fabrication of gas sensors with low working temperature is still highly desirable.

In this paper, a high-performance TEA sensor working at near room temperature (40 °C) is fabricated with Au/ZnO nanorods grown directly on flat Al_2O_3 substrates, which also simplified the traditional slurry-coating process for gas sensor fabrication. Au nanoparticles are decorated onto the ZnO nanorods by DC-sputtering under different deposition time of 5–20 s. The TEA sensor results indicate that the Au/ZnO composite nanorod sensor working 40 °C exhibits an ultrafast response (11 s), good stability, and a dramatic response enhancement in comparison with ZnO TEA sensor. The sensing performances and their gas sensing mechanism are discussed in detail in the following sections.

2. Experimental

2.1. Direct growth of ZnO and Au/ZnO nanorods on flat Al_2O_3 electrodes

All reagents were purchased from Sinopharm Chemical Reagent (Shanghai, China). The flat Al_2O_3 substrates were cleaned with acetone, ethanol, and deionized (DI) water by ultrasonication. The substrate is consisted with a pair of Au electrodes, Pt lead wires, and a heater (Fig. S1(a)). Fig. 1(a) schematically illustrates the fabrication process of ZnO nanorods sensor as well as Au/ZnO nanorods sensor. ZnO nanorods were synthesized via a low-temperature hydrothermal method as described below. 4.407 g zinc acetate dehydrate ($Zn(Ac)_2 \cdot 2H_2O$) was dissolved in 25 ml of ethylene glycol methyl ether with continuous stirring to get a clear solution. After that, cleaned flat Al_2O_3 substrates were immersed into the solution at room temperature for 2 h and then annealed at

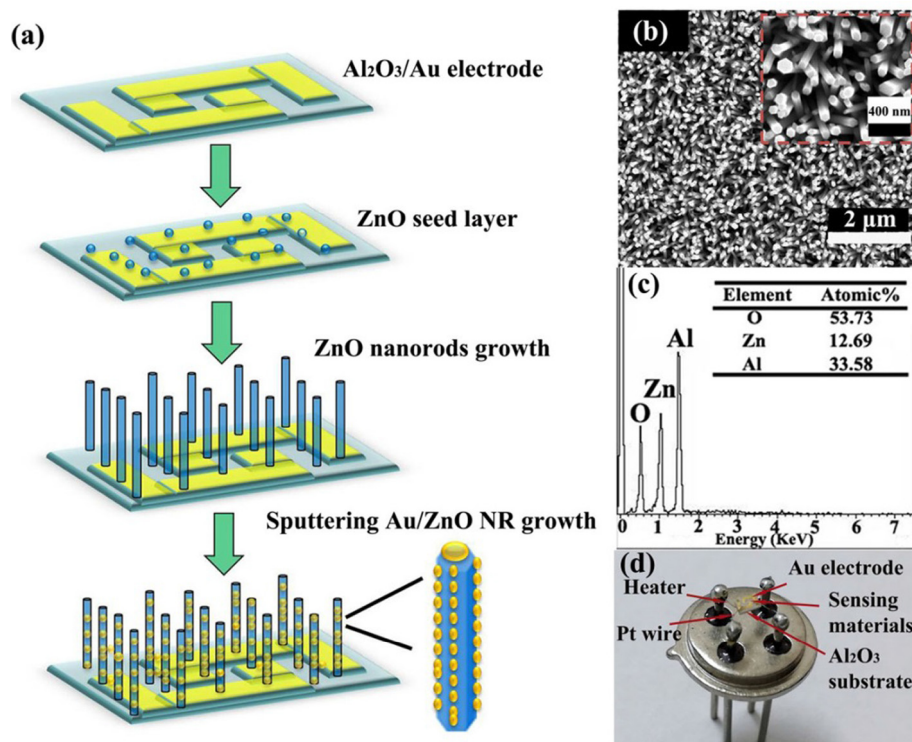


Fig. 1. (a) Schematic for the growth process of Au/ZnO nanorods; (b) SEM image of ZnO nanorods, inset is a local enlarged SEM image; (c) EDS spectrum of ZnO nanorods; (d) Optical image of gas sensor of ZnO nanorods fixed on an electronic bracket.

350 °C for 30 min to form a ZnO seed layer. A mixed aqueous solution of 0.025 M zinc nitrate and 0.025 M hexamethylenetetramine ($C_6H_{12}N_4$) was transferred into a Teflon-lined stainless steel autoclave. Afterward, flat Al_2O_3 substrates with seed layers were suspended into the above aqueous solution, heated to 95 °C for 3 h, and then cooled to room temperature. Finally, pure ZnO nanorods were obtained after several washings with deionized water and ethanol.

Au nanoparticles were decorated onto the ZnO nanorods by direct current (DC)-sputtering with different deposition time of 5 s, 10 s, 15 s, and 20 s. By controlling the sputtering times, the Au/ZnO nanorods heterostructure with different content of Au nanoparticles were obtained. Then, gas sensors were directly fabricated with ZnO nanorods, which was named as ZnO NR sensor. Another group of ZnO nanorods were further decorated with Au nanoparticles and the corresponding Au/ZnO gas sensor were named as Au/ZnO NR sensor (A, B, C, or D) for different Au nanoparticles sputtering time.

2.2. Material characterizations and sensor properties

The morphology microstructure and composition of ZnO and Au/ZnO nanorods were measured by a field emission scanning electron microscope (FESEM, FEI QUANTA FEG250) equipped with energy dispersive X-ray spectroscopy (EDS, INCA MAX-50) and a high-resolution transmission electron microscope (HRTEM, JEM-2100F, JEOL) with energy dispersive X-ray spectroscopy (EDS, Oxford Link-Isis). The phase of sensing materials was checked with X-ray diffraction (XRD, D8-Advance, Bruker) with $Cu K_{\alpha}$ radiation. The Brunauer-Emmett-Teller (BET) specific surface areas of the samples were examined through measuring the nitrogen adsorption-desorption isotherm (Micromeritics Instrument Corporation TriStar II 3020). The sensor properties were measured by a static gas-sensing test system (WS-60A, Weisheng Electronics, China). The measurement electronic circuit is shown in Fig. S1(b). The devices were put into an airproof test box. All the experiments were carried out with the relative humidity of 30% except when specially noted. Target gases such as TEA with calculated concentration were injected into the testing chamber by a microsyringe. The sensor response is defined as the ratio of R_a/R_g , where R_a and R_g are the resistances of the sensors in air and in target gas, respectively.

3. Results and discussions

3.1. Characterizations of ZnO and Au/ZnO nanorods

Fig. 1(b) is the SEM image of the pristine ZnO nanorods grown on flat Al_2O_3 substrates with predesigned electrical contacts. ZnO nanorods with uniform diameters stand vertically on the flat Al_2O_3 substrate. As shown in the inset of Fig. 1(b), the diameters of ZnO nanorods are about 60–70 nm. Fig. 1(c) represents the EDS spectrum of ZnO nanorods, and the O and Zn peaks can be clearly observed. The peak of Al also can be observed, which is attributed to the Al_2O_3 substrate. No additional impurity peaks are observed indicating the growth of pure ZnO nanorods. Fig. 1(d) is a typical optical photograph of ZnO gas sensor fixed on a electrical socket.

Fig. 2(a), (c), (e), and (g) are the SEM images of Au/ZnO nanorods with different gold sputtering time of 5 s, 10 s, 15 s, and 20 s, respectively. From the inset images we can see there are many Au particles randomly coating on the surface of ZnO nanorods and the nanorods surfaces become rough. With the increase of sputtering time, more Au particles are decorated onto the ZnO nanorods, and the concentration of Au further increases as proved

by the according EDS spectra shown in Fig. 2(b), (d), (f), and (h). It reveals that the atomic percentage of Au are about 0.28%, 0.56%, 1.06%, and 2.85%, respectively.

Fig. 3 shows the XRD spectrum of the as-synthesized ZnO and Au/ZnO NRs. All the diffraction peaks of spectrum (I) present a good match with typical hexagonal wurtzite structure of ZnO (JCPDS card 36-1451) [34] together with XRD peaks from Al_2O_3 substrate. When Au was deposited onto ZnO nanorods, the spectrum (II) of Au/ZnO NRs shows similar peaks with spectrum (I) and no additional XRD peak of Au nanoparticles could be observed due to their small loaded amount.

Fig. 4(a) shows a typical TEM image of a pristine ZnO nanorod, exhibiting 1D morphology with smooth surface. The selected-area electron diffraction (SAED) pattern in Fig. 4(b) reveals that the entire ZnO nanorod is of highly single-crystalline. Fig. 4(c) depicts the TEM image of typical Au/ZnO nanorods. Many small Au nanoparticles are loaded randomly onto the ZnO nanorods. Accordingly, the nanorods surface become rougher. The corresponding local enlarged TEM image is shown in the inset of Fig. 4(c), and the diameter of Au nanoparticles are about few nanometers. With HRTEM observation from Fig. 4(d), the lattice spacing of 0.260 nm and 0.235 nm corresponding to the ZnO (002) lattice planes and Au (111) lattice planes can be identified, respectively.

3.2. Sensing property comparisons of ZnO and Au/ZnO nanorods

The responses of ZnO NR sensor and four Au/ZnO NR sensors working at 40 °C for 50 ppm TEA are compared in Fig. 5(a) with the testing time change. All the Au/ZnO NR sensors exhibit much higher response than the ZnO NR sensor, which is closely related to the sputtered Au content. At beginning, with the increase of sputtering time, more Au particles are decorated onto the ZnO nanorods, which exhibits enhanced sensor performance. Under the optimized loading content, e.g. sample C, the device has the highest and fastest response (22–50 ppm TEA). However, if more Au nanoparticles are deposited onto the ZnO nanorods, a barrier against the TEA adsorption will form, which leads to the lower sensing property. Fig. 5(b) shows the sensor response evolution with operating temperatures changing from 40 to 200 °C. The maximum response of ZnO NR sensor to 50 ppm of TEA is only about 4 at 160 °C. But the Au/ZnO NR sensors exhibit higher responses than that of ZnO NR sensor at all temperatures, and it has reached a maximum value of 32 at 120 °C, which is due to the nanoscale structure of sensing materials. The diameters of ZnO nanorods are about 60–70 nm, and the diameter of Au nanoparticles are about few nanometers. The size reduction can accelerate the gas sensing reaction and thus reduce the operating temperature. In addition, the lower optimum working temperature is also related to the low C–N bond energy (307 kJ/mol), as TEA molecules can participate in the gas sensing reaction at relative low temperature [35]. When the working temperature is near room temperature (40 °C), the Au/ZnO NR sensor C response to 50 ppm of TEA is still up to 22. So, the following response curves were all measured at 40 °C to evaluate their sensing performance.

The sensor response characteristics based on the Au/ZnO NRs (A, B, C, and D) and pure ZnO NRs for TEA target gas of different concentration (1–200 ppm) at 40 °C are shown in Fig. 6(a). All of the sensor response increase with increasing TEA concentration. The response of Au/ZnO NR sensor C with optimized gold particles content increases more rapidly and exhibits the highest value compared with other sensors. Fig. 6(b) shows the sensor response repeatability after five cycles to 50 ppm TEA at 40 °C and all sensors exhibit good device repeatability.

The response-recovery time is also an important characteristic for gas sensor application. It is defined as the time taken by the sensor to achieve 90% of the total resistance change in the case

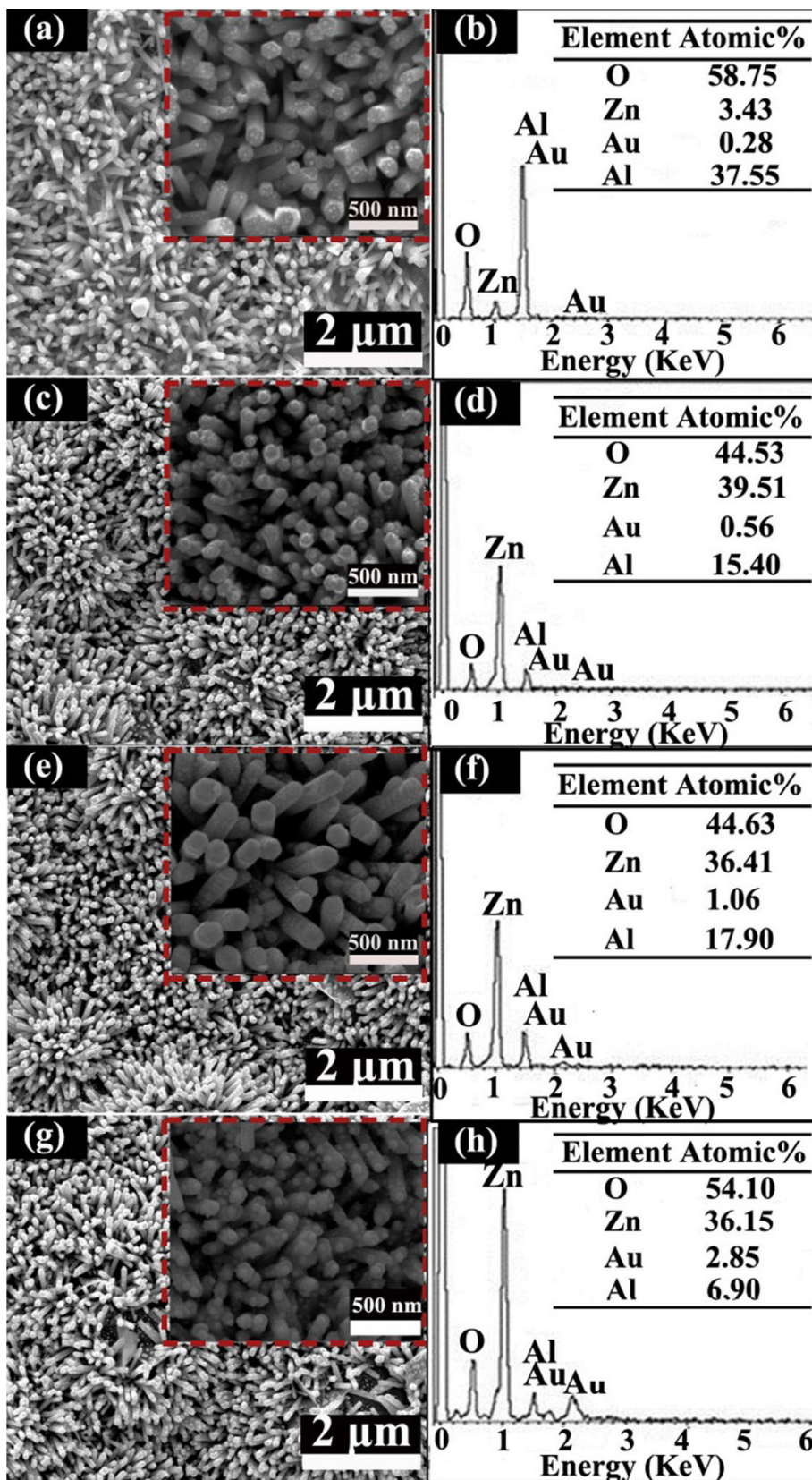


Fig. 2. SEM images of Au/ZnO nanorods directly grown on Al₂O₃ substrate under different sputtering time and their corresponding EDS spectra: (a) and (b): 5 s; (c) and (d): 10 s; (e) and (f): 15 s; (g) and (h): 20 s; the inset of (a), (c), (e), and (g) are a local enlarged SEM image.

of gas adsorption and desorption, respectively. Fig. 7(a) and (b) compare the response and recovery time of the two sensors to 50 ppm TEA at 40 °C. The response time of ZnO NR sensor and

the Au/ZnO NR sensor C are 10 s and 11 s, respectively. In addition, it shows that the recovery time of the Au/ZnO NR sensor C is 15 s, which is faster than that (21 s) of ZnO NR sensor. Due to the low

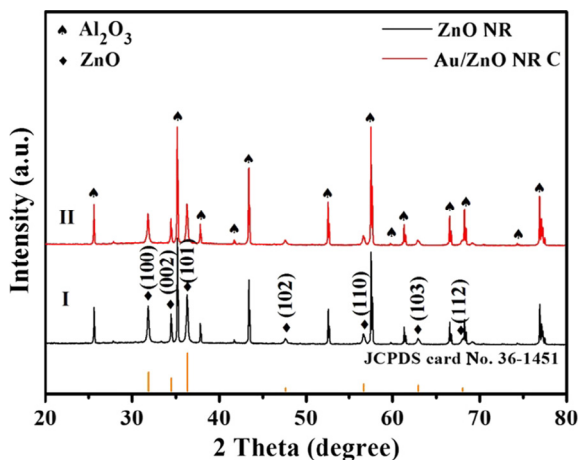


Fig. 3. The XRD spectra of the as-synthesised samples, (I) ZnO nanorods, and (II) Au/ZnO nanorods both on Al_2O_3 substrates.

working temperature, all sensors need a longer time to recover to a steady state. As it is known, chemical sensing at room temperature is hardly reversible because the thermal energy is usually lower than the activation energy for gas desorption, which leads to a long recovery time [36].

The device stability of two typical sensors over 40 days is tested as shown in Fig. 8(a). Clearly, both the sensors show nearly constant response to 50 ppm of TEA, which indicates good device stability. Moreover, for common sensor applications, environmental humidity is a prerequisite factor to be considered, which usually shows important influence on the sensor performance [37,38]. When the relative humidity (RH) changes from 30% to 76%, the ZnO NR sensor response almost keeps stable, as shown in Fig. 8(b). The Au/ZnO NR sensor C response decreases clearly when the relative humidity changed in the same range. However, it is still

higher than that of pristine ZnO NR sensor. The water molecules in the high RH environment are the main reason. First, the adsorption of water molecules leads to less chemisorption of oxygen species on the sensing material surface, which is responsible for the decreasing sensor response in high RH. Moreover, water molecules also act as a barrier against the TEA adsorption. Second, the reaction between the surface oxygen and the water molecules in high RH are conducive to a decrease in the sensor baseline resistance and result in a decrease of the response [1,39].

A comparison between the sensing performances of our Au/ZnO nanorod sensor and some previously reported TEA gas sensors is summarized in Table 1. As can be seen, the Au/ZnO nanorod sensor exhibits near room working temperature, lower detection limit, and relatively high response in our work. In addition, N_2 adsorption–desorption isotherms (Fig. S2) are used to calculate the specific surface areas of ZnO NRs and Au/ZnO NRs and their Brunauer–Emmett–Teller (BET) surface areas are determined to be 39.1343 and 20.5125 m^2/g , respectively, which clearly proves the formation of Au/ZnO heterostructure is the main reason for the improved sensor performance.

Fig. 9(a) summarizes the responses of ZnO NR sensor and Au/ZnO NR sensors with various TEA concentrations. Compared with other sensors, the response of the Au/ZnO NR sensor C increases significantly, and the sensor measured at 40 °C gets response values of 2.5 and 22.5 toward 1 and 50 ppm of TEA gas, respectively, which is about 11 times higher than that of the ZnO NR sensor. In addition, the gas responses of all sensors tend to saturate quickly. But, the Au/ZnO NR sensors exhibit better linear characteristic, as shown in Fig. 9(a) inset. Fig. 9(b) displays the responses of the five sensors to different gases of 50 ppm at 40 °C, e.g. TEA, ethanol, isopropyl alcohol, acetone, p-xylene, benzene, and ammonia. In all cases, the Au/ZnO NR sensor C has the highest response for TEA gas, which is about 7 times higher than that of the ZnO NR sensor. One possible reason is the different bond energies of target gas, for example, TEA (C–N), isopropyl alcohol (C–C), ethanol (O–H), benzene (C=C), acetone (C=O), and ammonia (N–H), are 307, 345, 458.8, 610.3,

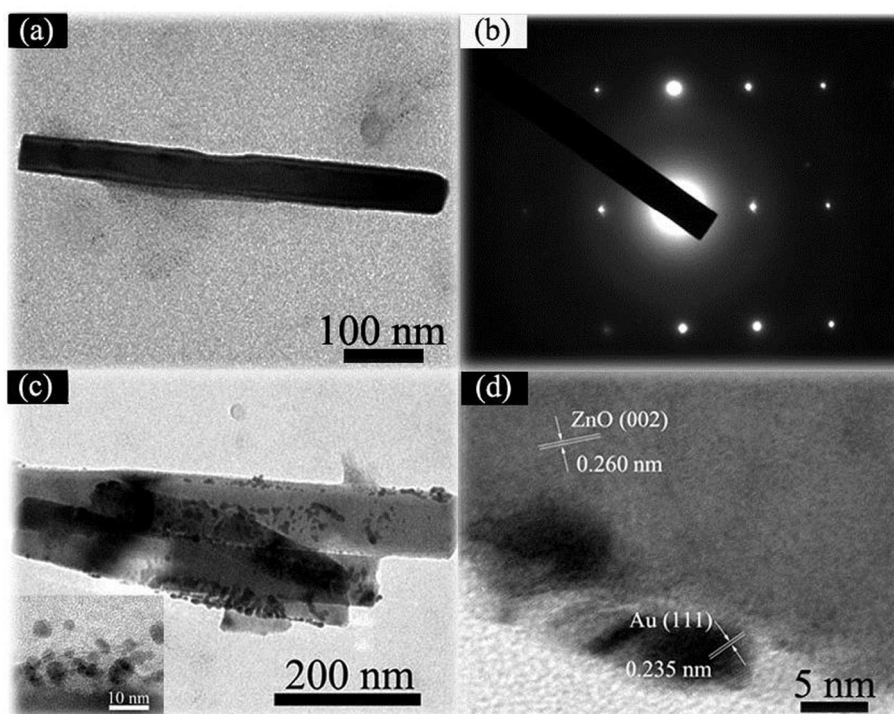


Fig. 4. (a) TEM image of a pristine ZnO nanorod; (b) SAED images of a typical ZnO nanorod in (a); (c) TEM image of Au/ZnO nanorods C, inset is a local enlarged TEM image; (d) HRTEM images of Au/ZnO nanorods C.

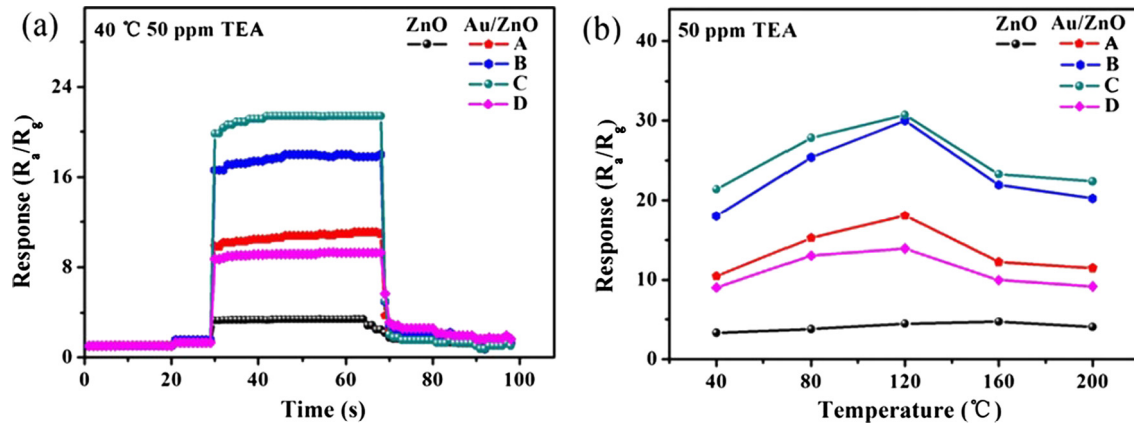


Fig. 5. (a) The typical response curves of five sensors (ZnO NR sensor, Au/ZnO NR sensor A, B, C, and D) to 50 ppm TEA at 40 °C under a relative humidity of 30%; (b) Responses of five sensors to 50 ppm TEA at different working temperature.

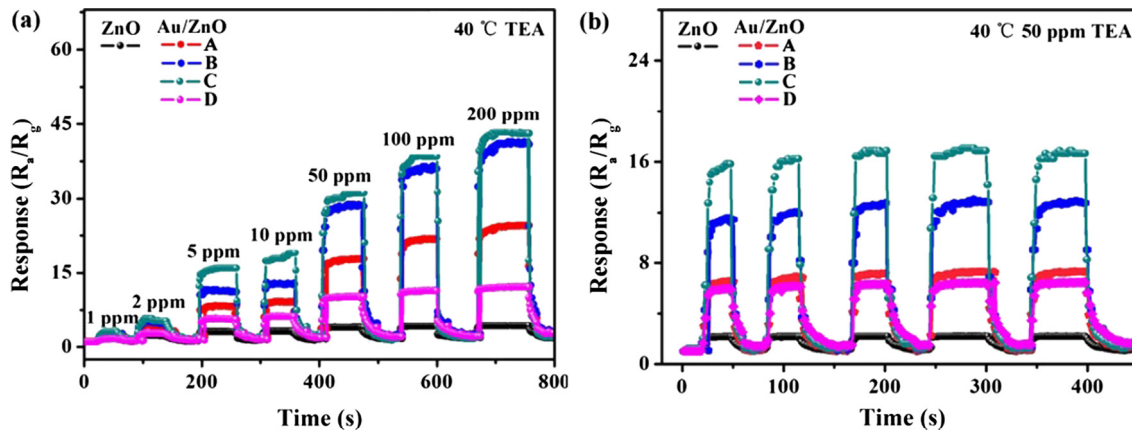


Fig. 6. (a) Response comparison of the ZnO NR sensor, and Au/ZnO NR sensors A, B, C and D to TEA of 1–200 ppm at 40 °C under a relative humidity of 30%; (b) The device repeatability of the five sensors to 50 ppm TEA at 40 °C.

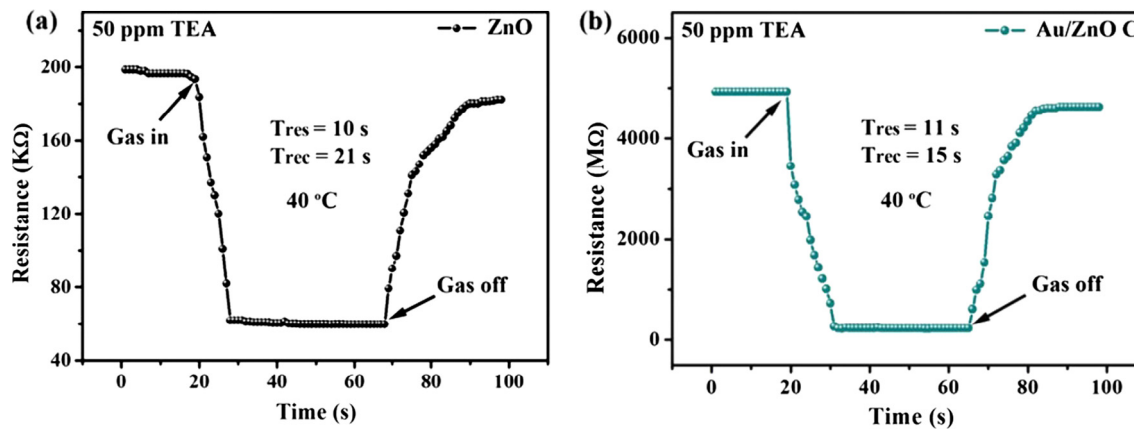


Fig. 7. The response-recovery curve of the (a) ZnO NR sensor and (b) Au/ZnO NR sensor C to 50 ppm TEA at 40 °C under a relative humidity of 30%.

798.9, and 391.5 kJ/mol, respectively [1,14,43]. Due to the low C–N bond energy, the high reaction activity of TEA molecules is beneficial to the high response of Au/ZnO NR sensors. Another possible reason is the catalytic effect of Au nanoparticles [1].

3.3. Gas sensing mechanism of Au/ZnO nanorods

The well accepted basic principle of n-type semiconductor sensors such as pure ZnO NR or film sensors is commonly described

with the surface depletion layer model [27,44], in which the surface resistance of n-type semiconductor is significantly swayed by the process of absorption and desorption of target gas molecules. Compared to the pure ZnO NR sensor, the sensing mechanism of Au/ZnO NR sensor is rather complex.

On the one hand, the work functions of ZnO and Au have been reported to be 4.45 eV [45] and 5.1 eV [46] as shown in Fig. 10(a) and their Fermi levels (E_F) are also different. Therefore, when ZnO semiconductor is contacting with the Au nanoparticles, the

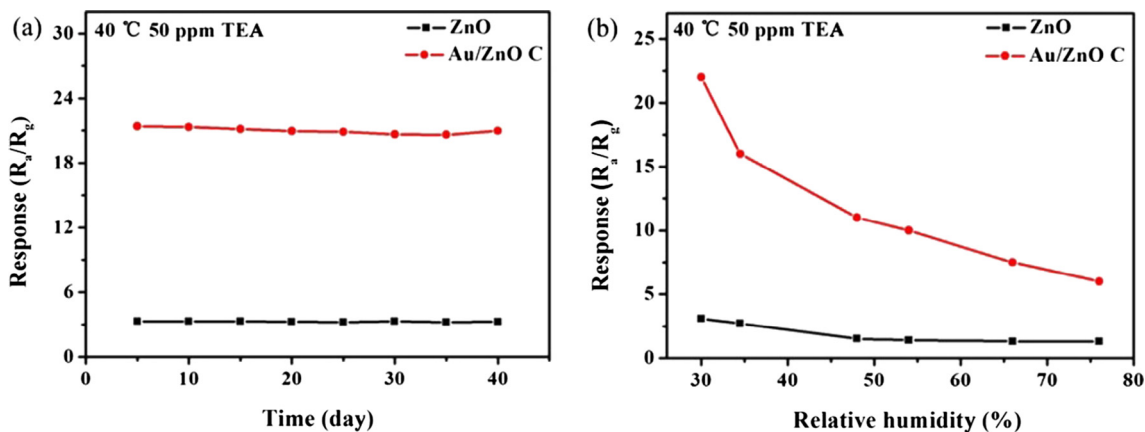


Fig. 8. (a) The stability measurement of the ZnO NR sensor and Au/ZnO NR sensor C to 50 ppm TEA at 40 °C; (b) The relationship between the sensor response and relative humidity.

Table 1

TEA sensing properties of our work and other reported oxide semiconductor gas sensors working under different operating temperatures.

Material	Gas concentration (ppm)	Operating temperature (°C)	Response (R_a/R_g)	Ref.
Au/ZnO nanorods	50	40	4	[1]
V ₂ O ₅ hollow spheres	100	370	7.3	[5]
Cr ₂ O ₃ microspheres	50	170	17	[9]
ZnO nanorods	500	150	300	[20]
α -Fe ₂ O ₃ nanorods	50	40	8.2	[35]
ZnO film	50	40	3	[40]
SnO ₂ flowerlike	100	350	4	[41]
ZnO micropyrramids	50	300	45	[42]
ZnO nanorods	50	40	2.5	Our work
Au/ZnO nanorods	50	40	22	Our work

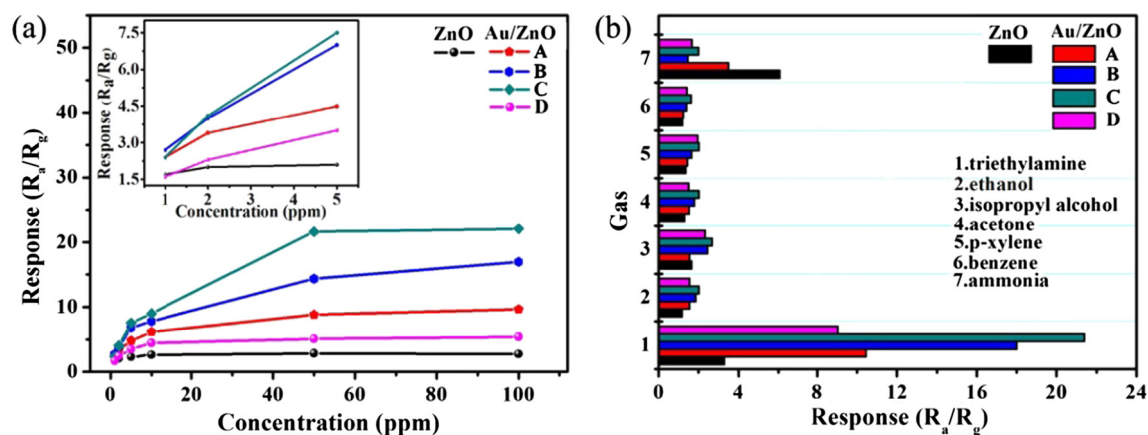
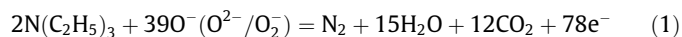


Fig. 9. (a) The corresponding relationship between the response and concentrations to TEA at 40 °C showing linear relationship over a wide concentration range. (b) gas response of the sensors to 50 ppm different tested gases at 40 °C.

electrons at higher E_F energy will transfer from the surface of ZnO to Au until the two Fermi energies equilibrate, which leads to the formation of Au/ZnO Schottky contact and widens the electron depletion layer on the ZnO NR surface [29,47,48] (Fig. 10b) and leads to a higher initial resistance state of Au/ZnO sensor than that of the pure ZnO nanorod sensor, as shown in Fig. 7. Considering that the ZnO NR can absorb oxygen molecules in air and combine with electrons to form negative oxygen ions $O_2^{\delta-}$ (O_2^- , O^- , O^{2-}) and an electron surface depletion layer, the discrete configuration of Au nanoparticles on the surface of ZnO NR will further extend the surface depletion layer as shown in Fig. 10(c). When Au/ZnO NR is exposed to TEA gas, the gas gets oxidized by negatively

charged oxygen ions and the electrons trapped by $O_2^{\delta-}$ ions automatically release back to Au/ZnO NR, which decreases the sensor resistance, shown in Fig. 10(d). The reaction between the $O_2^{\delta-}$ ions and TEA gas can be simply described as follows (reaction (1)) [14]



In brief, in comparison with the ZnO sensor, the formation of Schottky junction in Au/ZnO sensor greatly increases the resistance in air and decreases the resistance in TEA gas, as indicated in Fig. 7 (a and b). Thus, based on the definition of sensor response ($S = R_a/R_g$)

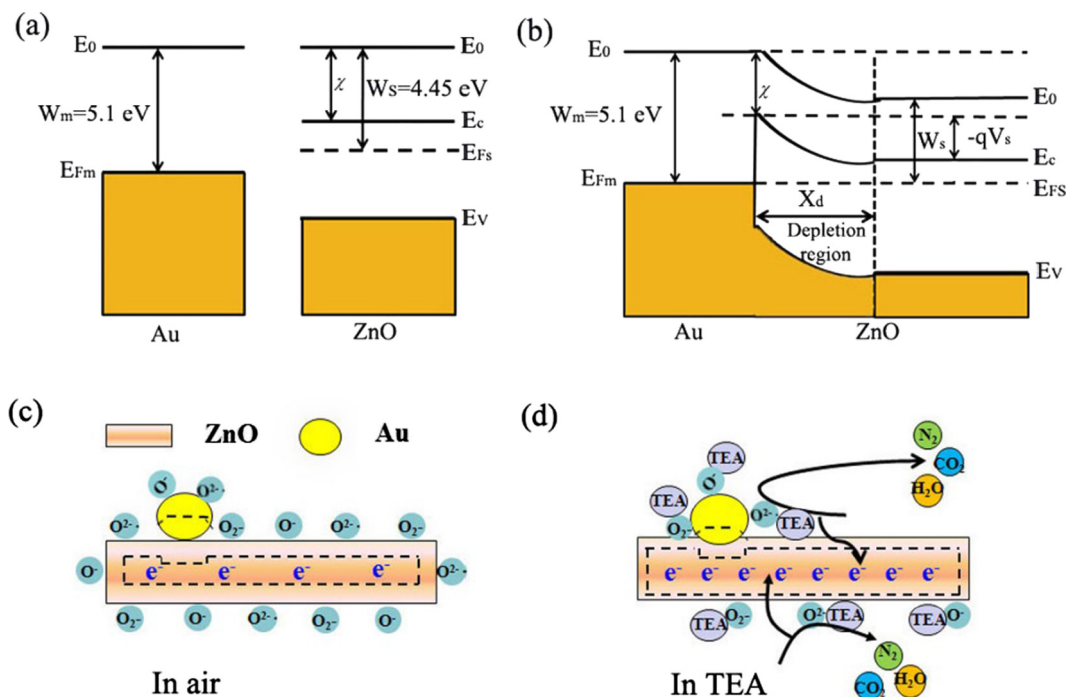


Fig. 10. (a) The energy band diagram of Au and ZnO; (b) The energy band diagram for metal/semiconductor junction of Au/ZnO heterostructure with a depletion region at the interface; (c) and (d) schematic model for the Au/ZnO NRs sensor exposed to air and TEA gas, respectively.

R_g), the enhanced response to TEA is mainly attributed to the variation of resistance caused by the formation of Au/ZnO Schottky junction. This theoretical model can also be used to explain other materials systems with their response improved by similar PN heterojunction, such as CuO-ZnO [33] and NiO-SnO₂ [14].

On the other hand, it is worth to noting that the use of noble metals, as an active component, can also improve sensor performance due to the catalytic effect of noble metals [49–51]. The Au nanoparticles on the ZnO nanorods can act as the centers for oxygen adsorption and decomposition, which can be described with reactions (2–3) during the sensor working. Obviously, Au as a catalyst promotes the decomposition of O₂ and increases the concentration of O⁻, which makes the reaction speed accelerate.



4. Conclusions

In summary, we report a low power sensitive TEA gas sensor working at near room temperature, by designing a Au/ZnO NR heterostructure, and discuss their sensing mechanism in detail. With the introduction of seed layers, ZnO NR grow directly on flat Al₂O₃ ceramic electrodes by a simple and cost-effective hydrothermal process. With sputtering method, the construction of Au/ZnO NR heterostructure is highly controllable and reproducible. Such gas sensor exhibits high response (22–50 ppm), lower detection limit (1 ppm) and good selectivity to TEA even at near room temperature (40 °C). The enhanced response to TEA gas molecules is basically attributed to the changes in resistance due to the formation of Schottky junction between Au nanoparticles and ZnO NRs. In addition, the catalysis of Au is also an significant reason to improve gas performance. This study of constructing metal/semiconductor provides a rational way for design and fabrication of the chemiresistance gas sensors with high performances.

Acknowledgment

This work is supported by NSFC (11174112) and Shandong Provincial Science Foundation (2014ZRB019JP). The research programs from Ministry of Education, China, are also acknowledged (213021A). BC thanks the Taishan Scholar Chaired Professorship tenured at University of Jinan.

Appendix A. Supplementary material

Supplementary data associated with this article can be found, in the online version, at <http://dx.doi.org/10.1016/j.jcis.2017.03.092>.

References

- [1] D.X. Ju, H.Y. Xu, Z.W. Qiu, Z.C. Zhang, Q. Xu, J. Zhang, J.Q. Wang, B.Q. Cao, *ACS Appl. Mater. Interfaces* 7 (2015) 19163–19171.
- [2] L. Xu, H. Song, J. Hu, Y. Lv, K. Xu, *Sens. Actuators, B* 169 (2012) 261–266.
- [3] L.-L. Sui, Y.-M. Xu, X.-F. Zhang, X.-L. Cheng, S. Gao, H. Zhao, Z. Cai, L.-H. Huo, *Sens. Actuators, B* 208 (2015) 406–414.
- [4] S.L. Bai, Y.Q. Ma, R.X. Luo, A.F. Chen, D.Q. Li, *RSC Adv.* 6 (2016) 2687–2694.
- [5] M. Wu, X. Zhang, S. Gao, X. Cheng, Z. Rong, Y. Xu, H. Zhao, L. Huo, *Cryst. Eng. Commun.* 15 (2013) 10123–10131.
- [6] J. Sun, X. Shu, Y. Tian, Z. Tong, S. Bai, R. Luo, D. Li, A. Chen, *Sens. Actuators, B* 238 (2017) 510–517.
- [7] T. Cai, L. Chen, Q. Ren, S. Cai, J. Zhang, *J. Hazard. Mater.* 186 (2011) 59–66.
- [8] H.Y. Yang, X.L. Cheng, X.F. Zhang, Z.K. Zheng, X.F. Tang, Y.M. Xu, S. Gao, H. Zhao, L.H. Huo, *Sens. Actuators, B* 205 (2014) 322–328.
- [9] J. Cao, Y. Xu, L. Sui, X. Zhang, S. Gao, X. Cheng, H. Zhao, L. Huo, *Sens. Actuators, B* 220 (2015) 910–918.
- [10] M.A. Lqbal, J.E. Szulejko, K.H. Kim, *Anal. Methods* 6 (2014) 5697–5707.
- [11] Y.H. Kim, K.H. Kim, *Anal. Chim. Acta* 780 (2013) 46–54.
- [12] Y.C. Chien, S.N. Uang, C.T. Kuo, T.S. Shih, J.F. Jen, *Anal. Chim. Acta* 419 (2000) 73–79.
- [13] W.H. Zhang, W.D. Zhang, *Sens. Actuators, B* 134 (2008) 403–408.
- [14] D.X. Ju, H.Y. Xu, Q. Xu, H.B. Gong, Z.W. Qiu, J. Guo, J. Zhang, B.Q. Cao, *Sens. Actuators, B* 215 (2015) 39–44.
- [15] J. Kim, K. Yong, *J. Phys. Chem.* 115 (2011) 7218–7224.
- [16] Y. Xiao, L. Lu, A. Zhang, Y. Zhang, L. Sun, L. Huo, F. Li, *ACS Appl. Mater. Interfaces* 4 (2012) 3797–3804.
- [17] X. Han, Y. Sun, Z. Feng, G. Zhang, Z. Chen, J. Zhan, *RSC Adv.* 6 (2016) 37750–37756.

- [18] A.L. Zou, Y. Qiu, J.J. Yu, B. Yin, G.Y. Cao, H.Q. Zhang, L.Z. Hu, *Sens. Actuators, B* 227 (2016) 65–72.
- [19] J. Guo, J. Zhang, M. Zhu, D.X. Ju, H.Y. Xu, B.Q. Cao, *Sens. Actuators, B* 199 (2014) 339–345.
- [20] Y.Z. Lv, C.R. Li, L. Guo, F.C. Wang, Y. Xu, X.F. Chu, *Sens. Actuators, B* 141 (2009) 85–88.
- [21] P. Rai, Y.S. Kim, H.M. Song, M.K. Song, Y.T. Yu, *Sens. Actuators, B* 165 (2012) 133–142.
- [22] Y.J. Chen, C.L. Zhu, G. Xiao, *Sens. Actuators, B* 129 (2008) 639–642.
- [23] L. Wang, Y. Kang, X. Liu, S. Zhang, W. Huang, S. Wang, *Sens. Actuators, B* 162 (2012) 237–243.
- [24] K. Shingange, Z.P. Tshabalala, O.M. Ntwaeaborwa, D.E. Motaung, G.H. Mhlongo, *J. Colloid Interface Sci.* 479 (2016) 127–138.
- [25] K.G. Girija, K. Somasundaram, A. Topkar, R.K. Vatsa, *J. Alloys Compd.* 684 (2016) 15–20.
- [26] W. Zhang, W. Zhang, *Sens. Actuators, B* 134 (2008) 403–408.
- [27] D.X. Ju, H.Y. Xu, Z.W. Qiu, J. Guo, J. Zhang, B.Q. Cao, *Sens. Actuators, B* 200 (2014) 288–296.
- [28] E. Filippo, D. Manno, A. Buccolieri, *Sens. Actuators, B* 178 (2013) 1–9.
- [29] L. Zu, Y. Qin, J. Yang, *J. Mater. Chem. A* 3 (2015) 10209–10218.
- [30] X. Li, X. Zhou, H. Guo, C. Wang, J. Liu, P. Sun, F. Liu, G. Lu, *ACS Appl. Mater. Interfaces* 6 (2014) 18661–18667.
- [31] S.M. Majhi, P. Rai, Y.T. Yu, *ACS Appl. Mater. Interfaces* 7 (2015) 9462–9468.
- [32] Y. Li, T. Lv, F. Zhao, Q. Wang, X. Lian, Y. Zou, *Electron. Mater. Lett.* 5 (2015) 890–895.
- [33] Q. Xu, D.X. Ju, Z.C. Zhang, S. Yuan, J. Zhang, H.Y. Xu, B.Q. Cao, *Sens. Actuators, B* 225 (2016) 16–23.
- [34] Z.W. Qiu, X. Yang, J. Han, P. Zhang, B.Q. Cao, Z. Dai, G. Duan, W. Cai, S. Bhandarkar, *J. Am. Ceram. Soc.* 97 (2014) 2177–2184.
- [35] Q. Xu, Z.C. Zhang, X.P. Song, S. Yuan, Z.W. Qiu, H.Y. Xu, B.Q. Cao, *Sens. Actuators, B* 245 (2017) 375–385.
- [36] Z. Fan, J.G. Lu, *Appl. Phys. Lett.* 86 (2005) 123510.
- [37] H. Hong, G.-S. Chung, *Sens. Actuators B* 195 (2014) 446–451.
- [38] Q. Qi, T. Zhang, Q. Yu, R. Wang, Y. Zeng, L. Liu, H. Yang, *Sens. Actuators, B* 133 (2008) 638–643.
- [39] Q. Qi, T. Zhang, S. Wang, X. Zheng, *Sens. Actuators, B* 137 (2009) 649–655.
- [40] S.H. Park, J.Y. Ryu, H.H. Choi, T.H. Kwon, *Sens. Actuators, B* 46 (1998) 75–79.
- [41] X. Zhou, Z.X. Xie, Z.Y. Jiang, Q. Kuang, S.H. Zhang, T. Xu, R.B. Huang, L.S. Zheng, *Chem. Commun.* 44 (2005) 5572–5574.
- [42] W.R. Li, H.Y. Xu, T. Zhai, H.Q. Yu, Q. Xu, X.P. Song, J.Q. Wang, B.Q. Cao, *J. Alloys Compd.* 695 (2017) 2930–2936.
- [43] L. Zhang, J. Zhao, H. Lu, L. Li, J. Zheng, J. Zhang, H. Li, Z. Zhu, *Sens. Actuators, B* 171–172 (2012) 1101–1109.
- [44] R.K. Sonker, S.R. Sabhajeet, S. Singh, B.C. Yadav, *Mater. Lett.* 152 (2015) 189–191.
- [45] Y.J. Fang, J. Sha, Z.L. Wang, Y.T. Wan, W.W. Xia, Y.W. Wang, *Appl. Phys. Lett.* 98 (2011) 033103.
- [46] U.T. Nakate, R.N. Bulakhe, C.D. Lokhande, S.N. Kale, *Appl. Surf. Sci.* 371 (2016) 224–230.
- [47] S. Lu, Q. Liao, J. Qi, S. Liu, Y. Liu, Q. Liang, G. Zhang, Y.T. Zhang, *Nano Res.* 9 (2015) 372–379.
- [48] L. Wang, H. Dou, Z. Lou, T. Zhang, *Nanoscale* 5 (2013) 2686.
- [49] N.S. Ramgir, P.K. Sharma, N. Datta, M. Kaur, A.K. Debnath, D.K. Aswal, S.K. Gupta, *Sens. Actuators, B* 186 (2013) 718–726.
- [50] F.B. Gu, H.H. Chen, D.M. Han, Z.H. Wang, *RSC Adv.* 10 (2016) 1039.
- [51] J. Lee, J.C. Park, J.U. Bang, *Chem. Mater.* 20 (2008) 5839–5844.